High Resolution Radar-based Occupancy Grid Mapping and Free Space Detection

6 authors, including:

Some of the authors of this publication are also working on these related projects:

autoMoVe View project

Automotive radar for HAD View project

High Resolution Radar-based Occupancy Grid Mapping and Free Space Detection

Mingkang Li[1,2], Zhaofei Feng[1], Martin Stolz[1], Martin Kunert[1], Roman Henze[2] and Ferit Küçükay[2]

[1]*Advanced Engineering Sensor Systems, Robert Bosch GmbH, Daimlerstr. 6, 71229, Leonberg, Germany*
[2]*Institute of Automotive Engineering, Technische Universität Braunschweig, Hans-Sommer-Str. 4, 38106, Braunschweig, Germany*

Keywords: Automotive Radar Sensor, Environmental Perception, Occupancy Grid, Free Space Detection, Imaging Radar.

Abstract: The high-resolution radar sensors have the ability to detect thousands of reflection points per cycle, which promotes the perception capability on a pixel level similar to video systems. In this paper, an occupancy grid map is created to model the static environment. The reflection amplitudes of all detection points are compensated, normalized, and then converted to the detection probability based on a radar sensor model. According to the movement of the ego vehicle, the a posteriori occupancy probability is computed to build the occupancy grid map. Thereafter the occupancy grid map is converted to the binary grid map, where the grids in the obstacle areas are defined as occupied. In order to eliminate the outliers, the connected occupied grids are clustered using the Connected-Component Labelling algorithm. Through the Moore-Neighbour Tracing algorithm the boundaries of the clustered occupied grids are recognized. Based on the boundaries, the interval-based free space detection is performed using the Bresenham's line algorithm. As mentioned, the occupancy grid map and the free space detection results obtained from radar road measurements match with the real scenarios.

1 INTRODUCTION

Taking the advantages of all-weather robustness, various applications with the radar sensors are found in the automotive industry, especially in the area of Advanced Driver Assistance Systems (ADAS). For instance, in Adaptive Cruise Control (ACC) system the radar sensors can detect objects within a wide range. After acquiring the value of object distance, the vehicle can be accelerated or decelerated automatically by the ACC system.

The development of ADAS towards Highly Automated Driving (HAD) improves continuously the demands on the high-resolution radar sensors. In order to handle complex applications and traffic situations, the radar sensors need a high angular and range resolution to capture enough environment information. Additionally, the high-resolution radar is required for the data fusion with the LiDAR or camera sensor on a pixel level.

The fast chirp linear Frequency-Modulated Continuous-Wave (FMCW) radar systems (Chirp Sequence radar) with an antenna array is already proved to be one of the most suitable solutions (Meinl et al., 2017). Because of the thousands of reflection points detected within one single measurement cycle, the environment perception ability of this radar system is at a high resolution level.

In the field of environment modelling with high resolution data, one of the common methods is occupancy grid mapping, which is originally known from probabilistic robotics (Moravec and Elfes, 1985) (Elfes, 1989). In this method, the environment is divided into a pattern of uniform grid cells, after which the detection points are filled into the corresponding grids. Instead of the points, the grids are tracked over time and hence the measurement noise and uncertainties are eliminated. At the same time, the probability of each grid cell being occupied is computed. This method is sufficient to model the static environment, because the reflection points from the static objects are detected at the same physical location in continuous measurement cycles and thus a stable occupancy grid map is achieved.

Based on the occupancy grid map, the free space zone can be recognized. For the vehicle trajectory

planning, the free space shall be estimated as precisely as possible, otherwise a collision with obstacles nearby may occur, especially after an evasive manoveur (Mouhagir et al., 2017).

The paper is organized as follows: Section 2 presents the state of the art in terms of the occupancy grid mapping and free space detection. Section 3 explains the used radar sensor and data preparation tasks like the coordinate system are explained. In Section 4, an approach of the occupancy grid mapping with the high resolution radar data is described. Based on the occupancy grid map, the algorithms required to detect the free space zone are presented in Section 5. Finally, a short summary for this paper is given.

2 STATE OF THE ART

In this section the works related to the occupancy grid mapping and free space detection are described.

2.1 Bayes' Theorem

Based on the Bayes' theorem, the new data in the current measurement cycle are combined with the previous data during the mapping of occupancy grid, in order to calculate the *a posteriori probability* over maps given the data: $p(m|R_{1:t}, V_{1:t})$, where m is the grid map, $R_{1:t}$ is the set of sensor measurement data from the time 1 to t, and $V_{1:t}$ the set of the vehicle position data from the time 1 to t.

$$\ell_t = log \frac{p(m|R_{1:t}, V_{1:t})}{1 - p(m|R_{1:t}, V_{1:t})} \qquad (1)$$

The log odds ratio of the a posteriori probability ℓ_t in the equation (1) can be computed as following

$$\ell_t = \ell_{t-1} + log \frac{p(m|R_t, V_t)}{1 - p(m|R_t, V_t)} - \ell_o, \qquad (2)$$

where $p(m|R_t, V_t)$ represents the *detection probability* processing the sensor data R_t and vehicle data V_t of the current measurement. The log odds ratio of the detection probability before processing any measurements ℓ_o is typically assumed as 0, since nothing is known about the surrounding environment before the first measurement.

2.2 Occupancy Grid Mapping

The occupancy grid mapping is previously implemented with the LiDAR sensor (Weiss,

Schiele, and Dietmayer, 2007) and camera sensor (Badino et al., 2008). With an advanced forward inverse sensor model, the reflection data from LiDAR sensor are converted to the occupancy probability, which is used as the detection probability in the Bayes' theorem (Nuss, 2017). If the LiDAR sensor detects an object, the grid, where the target is located, is recognized as occupied (see Figure 1). Between the occupied grid and LiDAR sensor, the grids within a certain radial distance to the LiDAR sensor are labelled as free. The occupancy probability of the grids over the distance threshold is computed with a linear function of the distance between the grids and the target. The grids (grey in Figure 1) without any measurement information are marked as unknown.
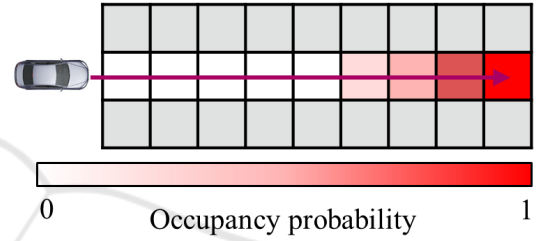

Figure 1: LiDAR sensor model.

Since the radar sensors can sense objects behind obstacles, a different sensor model is needed for the computation of the occupancy probability. Degerman, Pernstål and Alenljung (2016) extracted Signal-to-noise ratio (SNR) and computed the detection probability together with the Swerling 1 model. Using a static radar, Clarke et al. (2012) calculated the occupancy probability as a function of the reflection power, Fast Fourier Transform (FFT) bin number of the range, as well as the bearing. Werber et al. (2015) utilized the information about the Radar Cross Section (RCS) to develop the amplitude-based approach with occupancy grid mapping. Considering the different properties and modulations of the radar sensors, a general radar sensor model can be created by converting the reflection strength of the detection points into the occupancy probability.

Since the previous automotive radar sensors provide reflection data on the object level, the occupancy grid map is often created from multiple measurements in a limited area with the Simultaneous Localization and Mapping (SLAM) algorithm. Combining all the measurements, an occupancy grid map of the whole measured area is built, which helps to locate the vehicle position. The grid map is also used to classify the stored objects

on the cell level (Lombacher et al., 2017). However, this approach is not applicable for the occupancy grid mapping in the scope of real-time measurements.

2.3 Free Space Detection

Based on the occupancy grid map, the free space detection function is already developed in some previous works with the LiDAR and camera sensor.

With the LiDAR sensor model the free space is defined as a function of the distance between the sensor and the target (Homm et al., 2010). The further works focus on the road border recognition with the classification ability in terms of the camera sensor data (Badino, Franke and Mester, 2007) (Andrew and Isard, 1998). Konrad, Szczot and Dietmayer (2010) presented a road course estimation approach using a multilayer laser scanner. Lundquist, Schön and Orguner (2009) created a curve fitting method to detect the road boundary on the motorway. Schreier, Willert and Adamy (2016) developed a parametric free space map, which described a B-spline contour of arbitrarily shaped outer free space boundaries around the ego vehicle with additional attributes of the boundary type. In a complex vehicle environment, a large number of the curve parameters have to be estimated.

3 MEASUREMENT SETUP AND DATA PREPARATION

A developed high performance radar system is installed in the test vehicle and the measurement data are recorded. The ego vehicle motion model is simulated with the vehicle dynamic data from the Controller Area Network (CAN) bus. The coordinate systems of the vehicle and the grid map are adapted with each other.

3.1 Radar Sensor

A 77 GHz FMCW experimental high performance radar system is developed and mounted at the front of the vehicle (see Figure 2) (Li, 2017). A Chirp Sequence modulation with bandwidth B = 2.4 GHz, observation cycle time T = 50 ms and a 16 channel receive antenna array is applied.
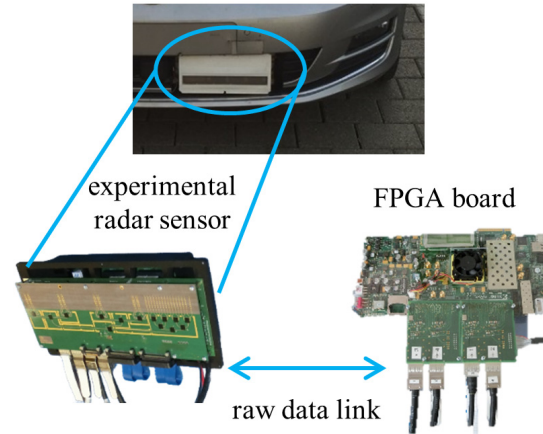

Figure 2: Experimental radar sensor and FPGA board.

The measured raw data dimensions are 4096 samples, 1024 ramps and 16 channels. A Field-Programmable Gate Array (FPGA) development board is used to realize the signal processing algorithms. A FFT over the samples is performed to determine the distance information (range) of detection points. For radial velocity detection, a second FFT over the ramps is computed. In these two dimensions a Chebyshev window is employed. An Ordered Statistics Constant False Alarm Rate (OS-CFAR) algorithm generates a threshold for the target extraction of the calculated two dimensional range-Doppler spectrum. The targets above the threshold level are processed and their directions (angle of arrival) are calculated with a Maximum Likelihood algorithm.

A velocity threshold is set to select the relevant target points from the static environment. The range and angle of the reflection points in the radar polar coordinate system are converted to $x_{r,i}$ and $y_{r,i}$ in the Cartesian coordinate system. The middle of the vehicle rear axle is defined as the origin point of the coordinate system. The reflection amplitude $A_{r,i}$ of each point is computed with the signal processing algorithm above. Thus, the information of reflection points R_t at the time t can be represented by

$$R_t = [x_{r,i}, y_{r,i}, A_{r,i}, t]^T, i \in 1 \dots N, \qquad (3)$$

where N is the number of the reflection points.

3.2 Vehicle Motion Model

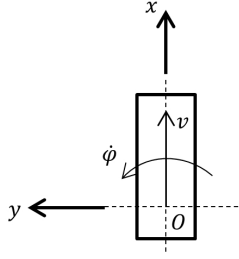Figure 3 shows the vehicle coordinate system defined by ISO 8855:2011.

Figure 3: Ego vehicle motion model.

From the CAN-Bus, the vehicle dynamic data like velocity v, acceleration a and turn rate $\dot\varphi$ are recorded. The ego vehicle motion is calculated based on the Constant Turn Rate and Acceleration (CTRA) model (Stellet et al., 2015) by

$$\begin{bmatrix} \dot{x} \\ \dot{y} \\ \dot{v} \\ \dot{\varphi} \end{bmatrix} = \begin{bmatrix} v \cdot cos(\varphi) \\ v \cdot sin(\varphi) \\ a \\ \dot\varphi \end{bmatrix}. \qquad (4)$$

By integrating equation (4), the ego vehicle position is calculated and presented by

$$V_t = [x_v, y_v, \varphi_v, t]^T. \qquad (5)$$

Based on the ego vehicle position, the grid map is tracked.

3.3 Grid Map Coordinate System

Generally the coordinate system of the occupancy grid map can be defined by two methods:

1) Ground-fixed coordinate system. The ego vehicle moves in this coordinate system at different points. This method is suitable for the measurement at limited place, like parking lot, otherwise a large grid map is recommended to ensure the ego vehicle is always in the map.

2) Vehicle-fixed coordinate system. The grid map is shifted and rotated to keep the origin point staying at the middle point of the vehicle rear axle. However, undesirable offsets appear during the shift and rotation. After the movement of the ego vehicle, one single grid in the past map may occupy several new grids in the shifted and rotated map, which makes the grid map unstable or inaccurate.

To model and visualize the environment around the vehicle in any places, the grid map coordinate system needs to move with the ego vehicle like in method 2. Meanwhile, some modifications are applied to solve the offset problem. According to the vehicle position, the grid map is just shifted with integer rows and columns in x- and y- direction. The rest difference between the origin point of the grid

map and the ego position x_v' and y_v' is retained (see Figure 4). The orientation of the grid map is fixed by using the ego vehicle direction from the first measurement. During the vehicle motion the grid map is not rotated, instead the orientation of the ego vehicle φ_v is saved. These values are used to update the points in the coordinate system of the grid map. With this method, the grid map is shifted in such a way, that no offset is caused during tracking grid map with the vehicle motion.

The length and width of the whole grid map is adapted with the detection range of the radar sensor. The size of a single grid is comparable with the resolution of the radar sensor.
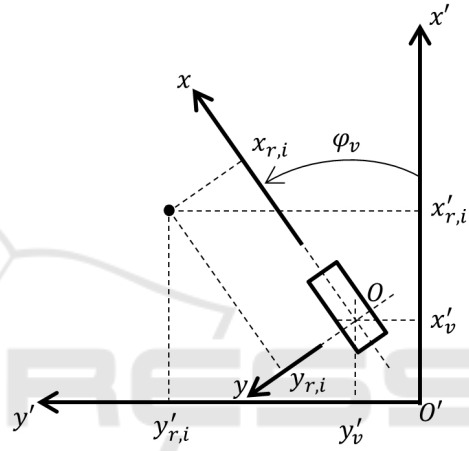

Figure 4: Grid map coordinate system.

The coordinates of the radar detection points in the coordinate system of the ego vehicle are converted into the grid map coordinate system by

$$\begin{bmatrix} x_{r,i}' \\ y_{r,i}' \end{bmatrix} = \begin{bmatrix} cos\varphi_v & -sin\varphi_v \\ sin\varphi_v & cos\varphi_v \end{bmatrix} \begin{bmatrix} x_{r,i} \\ y_{r,i} \end{bmatrix} + \begin{bmatrix} x_v' \\ y_v' \end{bmatrix}. \qquad (6)$$

4 OCCUPANCY GRID MAPPING

Depending on the position, the radar reflection points are assigned into the corresponding grids. In each time step, the occupancy grid is updated considering the current measured value by the radar sensor and the previous value of the grid. This leads to reduced measurement uncertainties and errors, since the real obstacles are typically detected in continuous measure cycles and mapped in the same grids over time.

The reflection strength of every new point is converted into a normalized value. Combining the values of all points in one single cell, the detection

probability in the cell is calculated. In each cycle this probability is computed and combined with each other to gain the a posteriori probability, which builds the final valid occupancy grid map. In the following part, the approach of the detection probability and a posteriori probability is introduced.

4.1 Detection Probability

In Figure 5, an image of one measurement cycle at a parking spot is shown, its corresponding bird's-eye view of the raw radar data is presented in Figure 6. In the next part, the reflection amplitudes of all detection points are converted to the detection probability in each grid.

Figure 5: Image of real scenario at a parking spot.
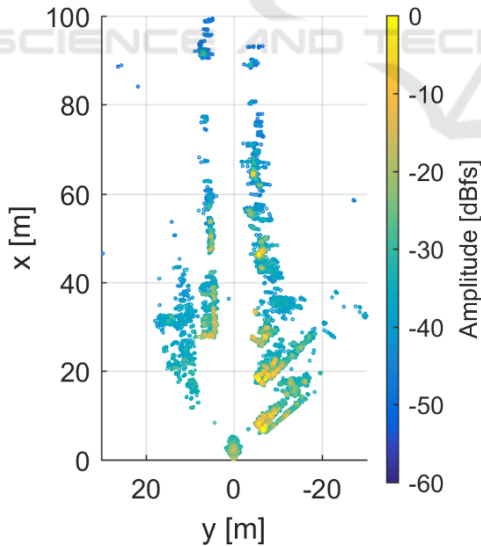
Figure 6: Bird's-eye view of radar reflection points.

4.1.1 Free-Space Loss Compensation

The free-space loss describes the decrease of the power density during the propagation of electromagnetic waves in free space according to the distance law, without taking additional attenuating factors (e.g. rain or fog) into account. The reflection amplitude is weakened with the increasing distance to the radar sensor.

In order to make the reflection strength and the converted detection probability of the obstacles independent of the distance, the free-space loss is compensated. The relationship between the reflection amplitude and the radial distance of the points is given in the equation (7). The amplitudes of all points are converted to the equivalent value $A_{r,i}{}^N$ at a reference distance d^N to the radar sensor.

$$A_{r,i}{}^N = A_{r,i} - 40 \, log_{10}\left(\frac{d'_{r,i}}{d^N}\right)$$

$$\text{with } d'_{r,i} = \sqrt{{x'_{r,i}}^2 + {y'_{r,i}}^2}$$

(7)

4.1.2 Antenna Gain Compensation

The reflection amplitudes of the points are additionally influenced by the angle between the target and the radar sensor, which is related to the antenna gain. The different antenna gain pattern is compensated, to achieve a reflection amplitude that is independent of the angle of arrival. In order to know the relationship between the amplitude and the angle of the reflection point, a corner reflector is placed at the same distance but with different angles to the radar sensor and the reflection amplitudes of the reflector at different angles are measured (see Figure 7). With this antenna pattern the amplitudes of all points are converted to an isotropic value that eliminates any angular dependency.
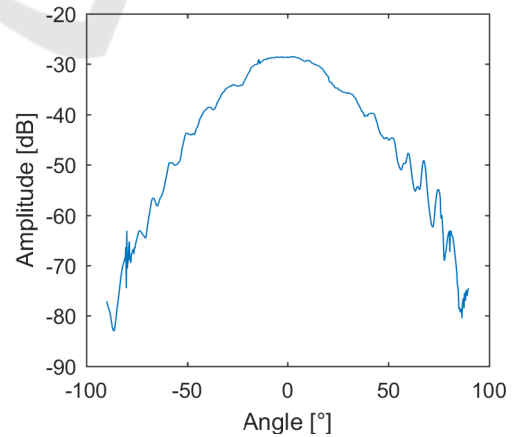

Figure 7: Antenna gain empirical characteristic curve.

4.1.3 Reflection Amplitude Normalization

The reflection amplitude is a relative value and

varies with different signal processing algorithms and parameters. However, the relationship of the amplitude between different points always presents the relative reflection strength. Therefore, the compensated amplitude is normalized to a value between 0 and 1. For each measurement cycle all the points are sorted by their amplitudes (see Figure 8).
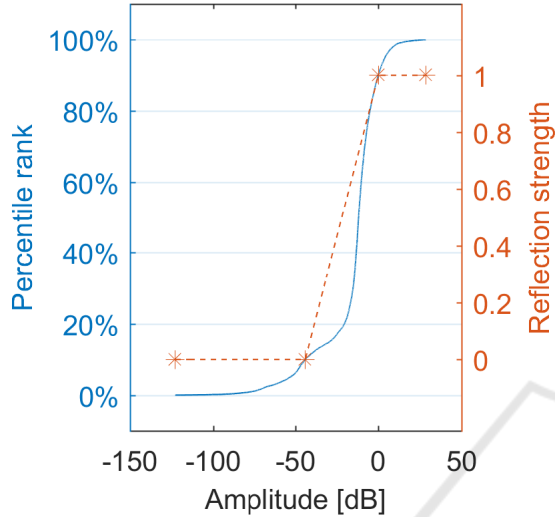

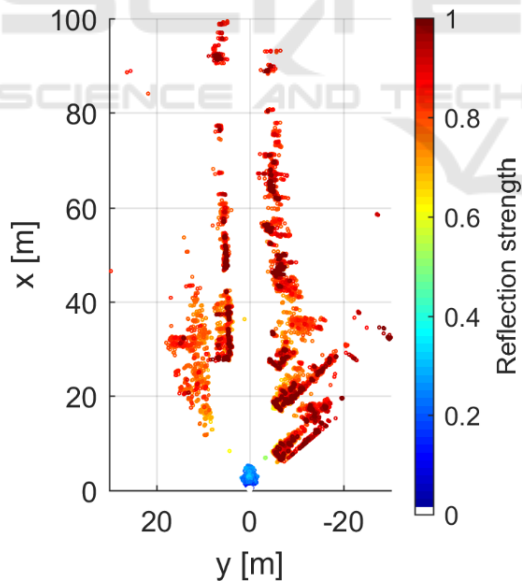Figure 8: Distribution and normalization of reflection amplitude.

Figure 9: Normalised reflection amplitude.

If the maximum amplitude value is set to 1 for the reflection strength and the minimum amplitude value to 0, an unsuitable scale is applied, since some points have an extreme value. Due to this, the 10% maximum value is normalized to 1 and the 10%

minimum value to 0. The reflection amplitude between them is converted according to a linear function to the value. Thus, the reflection strength of all points is normalized (see Figure 9).

4.1.4 Detection Probability in Single Grid

After the compensation and normalization of the reflection amplitude the points are allocated into the grids. Each grid can be occupied by several points with different reflection strength. The detection probability in one single grid can be calculated with the reflection strength of all points or the point number in this grid. In the grid some points with high reflection strength are detected from one object, while some points with a low reflection strength are reflected from another object nearby because of the antenna side lobes. The influence of those points with low reflection strength should be ignored, otherwise a low detection probability is computed by calculating the average reflection strength in one grid. Besides, the point number in every grid depends strongly on the size of the grid.

For the reasons above, only the points with 20% maximum reflection strength values in each grid are considered in the calculation. Their average reflection strength value is defined as the detection probability in the grid. In Figure 10 the detection probability of all grids in one measurement cycle is depicted.
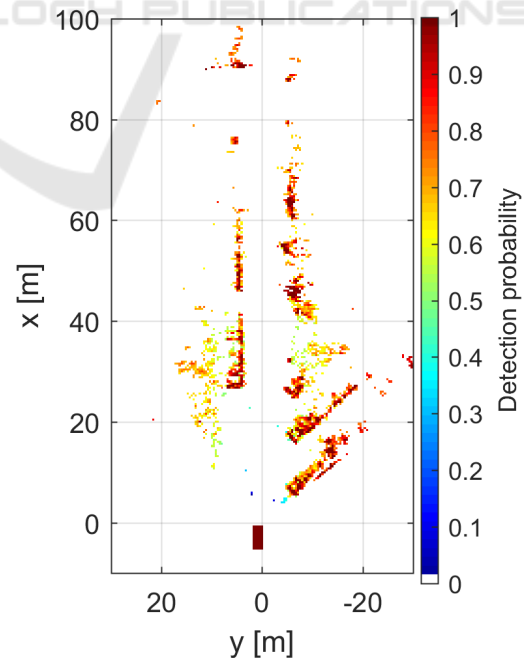

Figure 10: Detection probability (Ego vehicle is near origin point).

4.2 A Posteriori Probability

The radar sensor model converts the reflection strength to the detection probability, which is different from the LiDAR sensor model, so the equation (2) is modified.

At first, the detection probability is scaled to a value between 0.5 and 1 with the equation (8), otherwise the reflection strength under 0.5, which is also from the obstacles, leads to the reduction of the log odds ratio of the a posteriori probability.

$$p'(m|R_t, V_t) = 0.5 + 0.5 * p(m|R_t, V_t) \qquad (8)$$

However, with the scaling of the detection probability, the a posteriori probability is increased every time when the data from the new measurement cycle are calculated. This problem is solved by the degradation factor k. Then the log odds ratio of the a posteriori probability is computed with the equation

$$\ell_t = k * \ell_{t-1} + log \frac{p'(m|R_t, V_t)}{1 - p'(m|R_t, V_t)}. \qquad (9)$$

With the movement of the ego vehicle, the grids with the value of occupancy probability are shifted. Thus, the grid holds the detection probability based on the radar data in the current cycle and the occupancy probability in the previous cycles. The previous radar data should have less influence on the final occupancy probability than the new data. With the degradation factor k, the log odds ratio of the occupancy probability ℓ_{t-1} is reduced with respect to time. Therefore in each cycle the value of occupancy probability in the grids is reduced with the degradation factor at first and then increased with the current detection probability.

The log odds ratio ℓ_t in the grid is normalized to the value between 0 and 1, which indicates the a posteriori occupancy probability. The maximum and minimum limits are decided with a prognosis method: an object is located in one grid and detected with the same detection probability p_{th} in every cycle. After n measurement cycles, the grid is assumed to be 100% occupied. The current log odds ratio value is set to be upper limit $\ell_{th,max}$, which is represented by value 1 of the a posteriori probability. $\ell_{th,max}$ can be calculated by

$$\ell_{th,max} = \sum_{i=1}^{n} k^{i-1} * \log \frac{p_{th}}{1 - p_{th}}. \qquad (10)$$

In the following m cycles, no point with any reflection is detected in this grid. The grid is assumed to be free again. The current log odds ratio

value is defined as the lower limit $\ell_{th,min}$, which is represented by value 0 for the a posteriori probability. $\ell_{th,min}$ can be calculated by

$$\ell_{th,min} = \ell_{th,max} * k^m. \qquad (11)$$

The log odds ratio between the upper and lower limits is converted to the value between 0 and 1. In Figure 11 the change curve of the occupancy probability with the measurement cycle in the prognosis ($p_{th} = 0.9, n = m = 10$) is shown. In the 10th cycle the occupancy probability reaches the maximum value, then decreases and appears in the 20th cycle at the minimum.
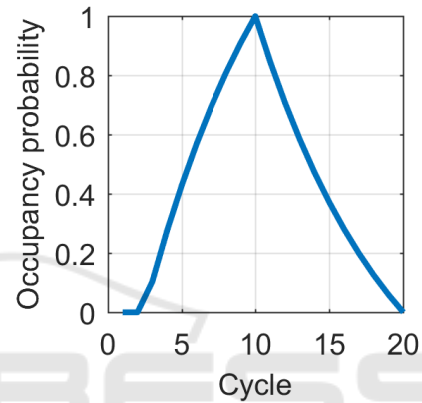

Figure 11: Change curve of occupancy probability in prognosis.
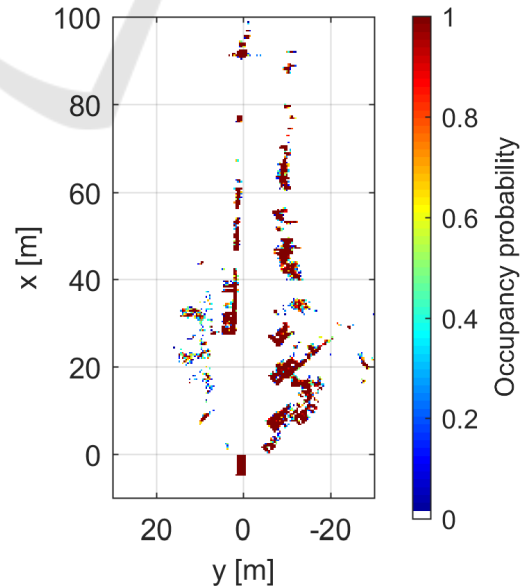
4.3 Results

Figure 12: Occupancy grid map at a parking spot.

The a posteriori probability stands for the final occupancy probability in each cycle. In Figure 12 the occupancy grid map from the measurement at a parking spot is shown, where several trucks and vans are parked (see Figure 5). In the occupancy grid map the contours of the trucks are recognized, although they are parked close to each other. The occupancy probability in the area of trucks is almost 1 and the grids between them have an occupancy probability of 0. This occupancy grid map represents correctly the static environment.

4.4 Amplitude Grid Mapping

The amplitude grid mapping is another common method to map the grid, which normalizes the maximum value of reflection amplitude over time in every grid into the occupancy probability. In Figure 13, an example of the amplitude grid mapping is shown. In contrast to the occupancy grid mapping, the measurement noise is not filtered and presented in the grid map, since only the maximum value is considered and the duration cycle of the measurement value is ignored. Because of the measurement noise, in some existing free space a high occupancy probability is computed, which disturbs the free space detection.
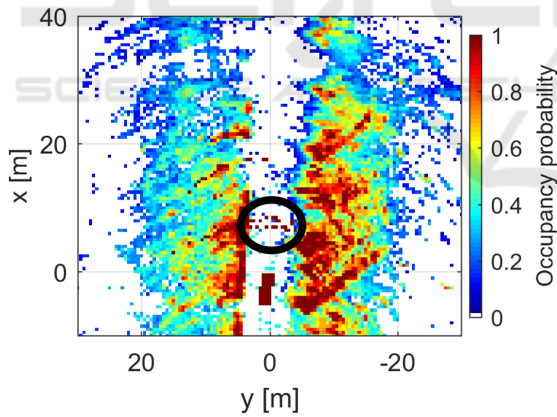

Figure 13: Example for amplitude grid mapping.

5 FREE SPACE DETECTION

The free space detection in the whole area around the vehicle is not achievable, because no data are captured out of the detection range and aperture of the radar sensor or behind some large obstacles. For the vehicle motion planning the field of interest (FOI) is the area along the possible trajectory. At first the occupancy status in all grids is determined

in order to create a binary grid map. With the clustering method, the occupied areas, which are caused by the constant and strong reflection points from the measurement errors, are defined as free space again. Based on the border recognition algorithm, the boundary of the occupied areas is detected, which realizes the free space detection along the vehicle trajectory.

5.1 Occupancy Status Determination

Before detecting the free space, it should be determined, whether the grids are occupied or not. The easiest way is to use a constant threshold of the occupancy probability, the occupancy status of the grids is decided, so that the occupancy grid map can be converted to a binary grid map (see Figure 14).
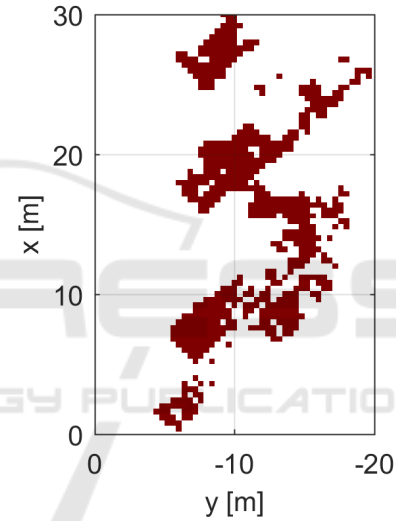

Figure 14: Binary grid map with threshold of occupancy probability (red: occupied grid, white: free grid).

However, the occupancy status of some grids has a mismatch with the respective value due to the features of the radar sensor and the OS-CFAR algorithm. From one object a lot of reflection points are detected and assigned in the different grids. Some points among them have low refection amplitudes, so that the occupancy probability of the corresponding grids is close to zero. Those grids are detected as free space, which actually belong to the obstacles. Here two methods are developed, in order to recognize the grids belonging to the obstacles but with low occupancy probability as occupied.

1) The grids with an occupancy probability lower than the threshold are considered. The amount of the grids in the neighbourhood, which have much higher occupancy probability than the selected grid, is calculated (see grids N in Figure 15, image on the

left). If this amount is larger than a threshold, the selected grid (gird C in Figure 15) is set to be occupied. Using this method, the grids with a lower occupancy probability in the inside and border area of obstacles are recognized as occupied.

2) The grids with zero occupancy probability are handled. If the two "sandwiched" grids (see grids N in Figure 15, middle and right) have a high occupancy probability and are declared as occupied, the selected grid is set to be occupied. Thus, especially the grids with zero occupancy probability in the inside area of obstacles are detected as occupied.
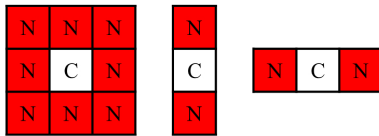

Figure 15: Neighbour grids (C: centre grid. N: neighbour grid).

Using the methods above, the occupancy status of all grids can be determined. An example of the results is shown in Figure 16.
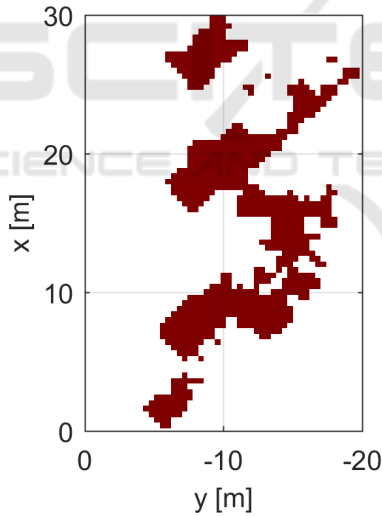

Figure 16: Processed binary grid map.

5.2 Clustering Binary Grids

With the occupancy grid mapping, the random measurement noise is filtered. However, some reflection points are caused by the strong objects nearby or the measurement errors. In the binary grid map the points usually occupy some areas with small size outside the obstacles, which are named as outliers. Using the threshold of the connected occupied area size, the outliers are filtered.

In order to calculate the size of the connected occupied areas, it is necessary to group the binary grids at first. Three popular clustering algorithms are discussed here:

1) K-Means (Lloyd, 1982). The partitions of the grids are divided into a predefined number of clusters in which each grid belongs to the cluster with the nearest mean. Since the environment around the vehicle changes all the time, it is not efficient to predefine the number of clusters.

2) Density-Based Spatial Clustering of Applications with Noise (DBSCAN) (Ester et al., 1996). The grids are grouped together and classified into core, border and noise grids depending on the number of occupied neighbour grids. The noise grids here are recognized as outliers. In order to filter the noise grids precisely, a relative low distance threshold between the grids and a relative high threshold of the grid number is selected. However, the calculation time is very long, because it is a quadratic function of the grid number in the worst case.

3) Connected component labelling (CCL) (Rosenfeld and Pfaltz, 1999) (He, Chao and Suzuki, 2008). The connected occupied grids in binary grid map is detected and clustered. It is not necessary to predefine any parameters. Additionally it takes significantly less computational burden than DBSCAN. For this reason, CCL is chosen as the clustering algorithm here.
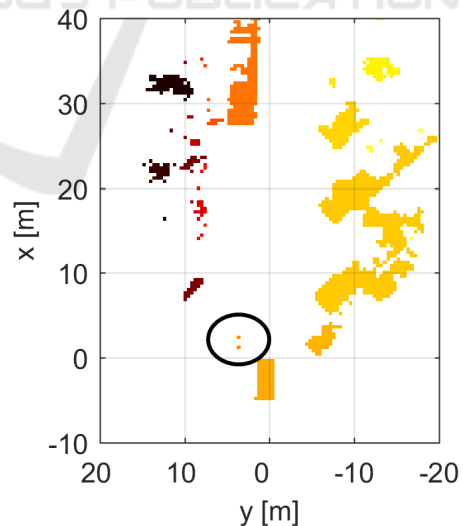

Figure 17: Clustering with CCL algorithm.

The number of the grids in each cluster is calculated. With a number threshold the outliers are found and the grids from the outlines are marked as free again. This processing step is meaningful,

because some outliners are located directly in front of the vehicle, where belongs to the FOI. In Figure 17 an example of the clustering result with CCL algorithm is demonstrated. The grids in the black circle are clustered and then defined as free again.

5.3 Border Recognition

The boundaries of the clustered and occupied binary grids are mostly relevant for the free space detection. The Moore-Neighbour Tracing (MNT) algorithm is introduced here to recognize the border of the occupied areas (Gonzalez et al., 2004). In Figure 18 the MNT algorithm is described. Starting from a random occupied grid B1, the next occupied neighbour grid in the clockwise direction B2 is searched. The iteration loop terminates when the initial grid is visited for a second time.
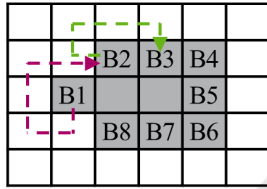

Figure 18: MNT Algorithm (B: border grid).

All reached grids are labelled as border grids, which helps to detect the free space along the trajectory. In Figure 19 an example of the border recognition result is shown.
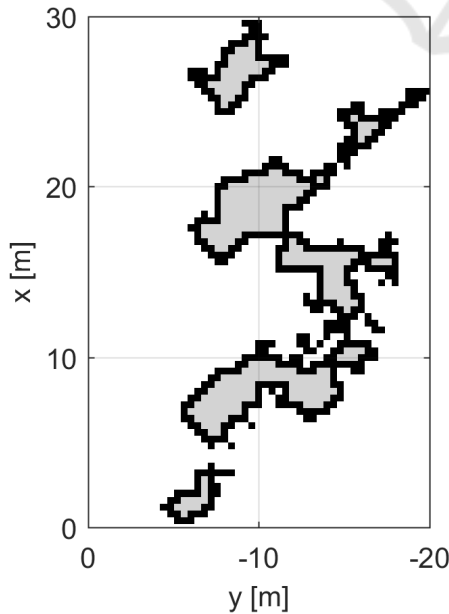

Figure 19: Border recognition (black: border grid, grey: occupied grid).

5.4 Interval-based Free Space Model

The free space along the vehicle trajectory is defined by the narrowest distance between the vehicle future possible position and the border of the occupied areas.

At first the trajectory of the ego vehicle is calculated with the current dynamic data based on the CTRA model, where the vehicle positions and orientations along the trajectory are computed. It is also possible to calculate the vehicle trajectory with any manoeuvres. The vehicle trajectory is defined as baseline and extended with a certain distance considering the orientation at each position to an area, which is similar to a sector and defines the FOI along the trajectory (see Figure 20).
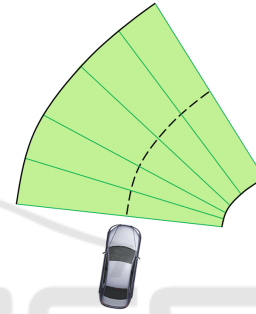

Figure 20: FOI and intervals along the trajectory.

Thereafter the FOI is divided into intervals with a certain length along the trajectory. The interval is always perpendicular to the vehicle orientation at each point. The length of one single interval is defined as a function of the vehicle velocity, because a wider free space is needed with increasing velocity.

In order to realize the interval-based free space model, the grids, in which the vehicle positions in the FOI are located, are selected to be the baseline grids. The grids on the left and right side of the baseline grids are visited with the Bresenham's line algorithm, which is located in the perpendicular direction to the vehicle orientation at each position (see Figure 21).
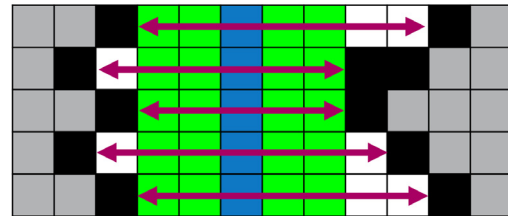

Figure 21: Free space detection in one interval (Blue: baseline grid, green: free space grid, black: border grid, grey: occupied grid).

The occupied grid with the smallest distance to each baseline grid is searched. Then this distance is defined as the width of the free space interval. The grids in the interval, which are closer to the baseline grids, are labelled as free space. Similarly, the width of all the intervals can be calculated, so that the free space along the vehicle trajectory is detected.

5.5 Results

In Figure 22 an example of the free space detection at the parking spot is shown. On the left side in front of the vehicle, more free space exists than on the right side, which means, the evasive trajectory to left is more feasible than right. Additionally the parking slots between the trucks are recognized as free space, which helps to generate the parking manoeuvre.
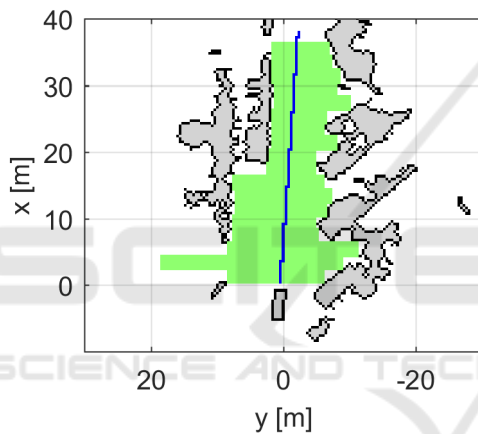
Figure 22: Example for free space detection.

In Figure 23 and Figure 24 another example on the public road is shown. There are several warning posts at the left side of the road, which are separately detected as obstacles in the map. The distance between the warning posts is recognized as free space.

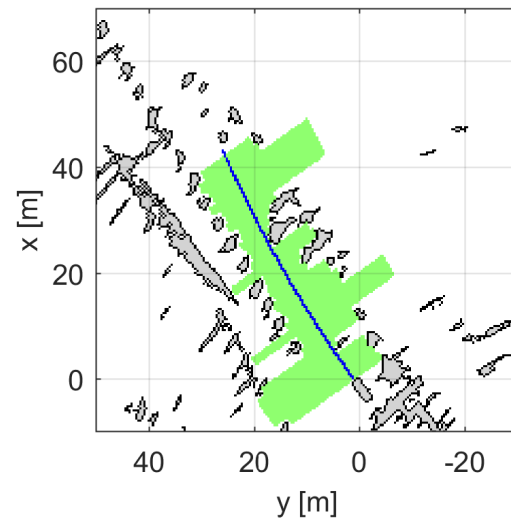Figure 23: Image for measurement on public road.

Figure 24: Free space detection on public road.

6 CONCLUSIONS

This paper presents an approach of the occupancy grid mapping and free space detection based on the high resolution radar sensors.

The positions and reflection amplitudes of the target points are detected with radar sensor and used as input data for the occupancy grid mapping. The reflection amplitudes are compensated according to the free-space loss and antenna pattern gain, and finally normalized. Based on the positions, the detected points are assigned to the corresponding grids. The detection probability of the individual cells is calculated as the function of the reflection strength of the detection points. With the movement of the ego vehicle, the value of the grids is degraded and then combined with the new data to compute the a posteriori occupancy probability. Thus, an occupancy grid map is updated over the course of time.

Thereafter the occupancy grid map is converted to the binary grid map. The grids in the obstacle areas are searched and labelled as occupied depending on the neighbour grids. Using the CCL algorithm, the connected occupied grids are clustered, in order to eliminate the outliers. With the MNT algorithm the border of the clustered occupied grids is recognized. Finally an interval-based free space is detected utilizing the Bresenham's line algorithm. According to the measurement results the detected free space and obstacles with the approach above match with the real scene.

ACKNOWLEDGEMENTS

REFERENCES

Andrew, B. and Isard, M., (1998). *Active Contours: The Application of Techniques from Graphics, Vision Control Theory and Statistics to Visual Tracking of Shapes in Motion*. 1st ed. London: Springer.

Badino, H., Franke, U. and Mester, R., (2007). Free Space Computation Using Stochastic Occupancy Grids and Dynamic Programming. In *International Conference on Computer Vision (ICCV), Workshop on Dynamical Vision*, Rio de Janeiro.

Badino, H., Mester, R., Vaudrey, T., Franke, U. and Daimler AG, (2008). Stereo-based Free Space Computation in Complex Traffic Scenarios. In *IEEE Southwest Symposium on Image Analysis and Interpretation (SSIAI),* Santa Fe, pp. 189-192.

Clarke, B., Worrall, S., Brooker, G. and Nebot, E., (2012). Sensor Modelling for Radar-Based Occupancy Mapping. In *IEEE/RSJ International Conference on Intelligent Robots and Systems (IROS)*, Vilamoura, pp. 3047-3054.

Degerman, J., Pernståhl, T. and Alenljung, K., (2016). 3D Occupancy Grid Mapping Using Statistical Radar Models. In *IEEE Intelligent Vehicles Symposium (IV),* Gothenburg, pp. 902-908.

Elfes, A., (1989). Using Occupancy Grids for Mobile Robot Perception and Navigation. In *Computer*, vol. 22, no. 6, pp. 46-57.

Ester, M., Kriegel, H. P., Sander, J. and Xu, X., (1996). A Density-Based Algorithm for Discovering Clusters in Large Spatial Databases with Noise. In *Proceedings of the Second International Conference on Knowledge Discovery and Data Mining*, Portland, pp. 226-331.

Gonzalez, R. C., Woods, R. E. and Eddins, S. L., (2004). *Digital Image Processing Using MATLAB*, Lexington: Pearson Prentice Hall.

He, L., Chao, Y. and Suzuki, K., (2008). A Run-Based Two-Scan Labeling Algorithm. *IEEE Transactions on Image Processing*, 17(5), pp. 749-756.

Homm, F., Kaempchen, N., Ota, J. and Burschka, D., (2010). Efficient Occupancy Grid Computation on the GPU with LiDAR and Radar for Road Boundary Detection. In *IEEE Intelligent Vehicles Symposium (IV)*, San Diego, pp. 1006-1013.

Konrad, M., Szczot, M. and Dietmayer, K., (2010). Road Course Estimation in Occupancy Grids. In *IEEE Intelligent Vehicles Symposium (IV)*, San Diego, pp. 412-417.

Li, M., (2017). High-Resolution Radar Based Environment Perception and Maneuver Planning. In *CTI Symposium on Automated Driving, Future Mobility and Digitalization (ADFD)*, Hannover.

Lloyd, S., (1982). Least Squares Quantization in PCM. *IEEE Transactions on Information Theory*, 28(2), pp. 129-137.

Lombacher, J., Laudt, K., Hahn, M., Dickmann, J. and Wöhler, C., (2017). Semantic Radar Grids. In *IEEE Intelligent Vehicles Symposium (IV)*, Los Angeles, pp. 1170-1175.

Lundquist, C., Schön, T. B. and Orguner, U., (2009). Estimation of the Free Space in Front of a Moving Vehicle. In *SAE World Congress & Exhibition*, Detroit.

Meinl, F., Stolz, M., Kunert, M. and Blume, H., (2017). An Experimental High Performance Radar System for Highly Automated Driving. In *IEEE MTT-S International Conference on Microwaves for Intelligent Mobility (ICMIM)*, Nagoya, pp. 71-74.

Moravec, H. and Elfes, A., (1985). High Resolution Maps from Wide Angle Sonar. In *Proceedings of IEEE International Conference on Robotics and Automation*, St. Louis, pp. 116-121.

Mouhagir, H., Cherfaoui, V., Talj, R., Aioun, F. and Guillemard, F., (2017). Using Evidential Occupancy Grid for Vehicle Trajectory Planning Under Uncertainty with Tentacles. In *IEEE 20th International Conference on Intelligent Transportation Systems (ITSC),* Yokohama.

Nuss, D. (2017). *A Random Finite Set Approach for Dynamic Occupancy Grid Maps*. PhD. University of Ulm.

Rosenfeld, A. and Pfaltz, J. L., (1999). Sequential Operations in Digital Picture Processing. *Journal of the ACM*, 13(4), pp. 471-494.

Schreier, M., Willert, V. and Adamy, J., (2016). Compact Representation of Dynamic Driving Environments for ADAS by Parametric Free Space and Dynamic Object Maps. *IEEE Transactions on Intelligent Transportation Systems*, 17(2), pp. 367-384.

Stellet, J. E., Straub, F., Schumacher, J., Branz, W. and Zöllner, J. M., (2015). Estimating the Process Noise Variance for Vehicle Motion Models. In *IEEE 18th International Conference on Intelligent Transportation Systems (ITSC)*, Las Palmas, pp. 1512-1519.

Weiss, T., Schiele, B. and Dietmayer, K., (2007). Robust Driving Path Detection in Urban and Highway Scenarios Using a Laser Scanner and Online Occupancy Grids. In *IEEE Intelligent Vehicles Symposium (IV)*, Istanbul, pp. 184-189.

Werber, K., Rapp, M., Klappstein, J., Hahn, M., Dickmann, J., Dietmayer, K. and Waldschmidt, C., (2015). Automotive Radar Gridmap Representations. In *IEEE MTT-S International Conference on Microwaves for Intelligent Mobility (ICMIM)*, Heidelberg, pp. 1-4.